Correlations between microphysical properties of large-scale semi-transparent cirrus from TOVS and the state of the atmosphere from ECMWF ERA-40 reanalyses

G. Rädel, C. J. Stubenrauch, F. Eddounia

C. N. R. S. / IPSL Laboratoire de Météorologie Dynamique, Ecole Polytechnique, 91128 Palaiseau cédex, France

Introduction

Cirrus clouds (semi-transparent ice clouds) cover about 30% of the globe (e. g., Wylie and Menzel, 1999). Their radiative effect due to changes of their microphysical properties can vary significantly (e.g., Kristjansson et al., 2000). In General Circulation Models these microphysical properties, such as dominating ice crystal shape and sizes, must be predicted from available macrophysical quantities, such as temperature, ice water path and winds (e. g. McFarlane et al., 1992; Donner et al., 1997; Kristjansson et al., 1999). Most utilised relationships have been established only for a few places on earth and for very limited time periods (e. g. Heymsfield and Platt, 1984; McFarquar and Heymsfield, 1996; Korolev et al., 2001). The use of satellite observations allows one to obtain a more coherent image of the validity of these correlations found in regional field campaigns.

Since 1979, the TIROS-N Operational Vertical Sounder (TOVS) instruments (Smith et al., 1979) aboard the NOAA Polar Orbiting Environmental Satellites have measured radiation emitted and scattered from different levels of the atmosphere, and therefore are an important tool for a continuous survey of the state of the atmosphere over the whole globe. Their relatively high spectral resolution yields reliable cirrus properties, day and night (e.g., Wylie et al., 1994, Stubenrauch et al., 1999a). Mean effective ice crystal diameters, D_e, of cirrus clouds are retrieved by taking advantage of the fact that spectral cirrus emissivity differences between 11and 8 μm depend on this parameter (Stubenrauch et al., 1999b; Rädel et al., 2003). This method is sensitive to diameters up to 80 μm, and is applied to large-scale semi-transparent cirrus (visible optical thickness between 0.7 and 3.8). Ice water path (IWP) is then determined from the cirrus emissivity at 11 μm and the retrieved D_e. The averages of these quantities over the globe from 60°N to 60°S are 55 μm and 30 gm^{-2}, respectively.

In this article we study seasonal and regional variations of these quantities as well as correlations with atmospheric properties. Therefore, atmospheric humidity and dynamical properties of the atmosphere, such as horizontal and vertical winds, have been extracted from the ERA-40 reanalyses of the European Centre for Medium Range Weather Forecasts (ECMWF).

Cloud properties from TOVS Path-B

The TOVS system consists, in particular, of two sounders: the High resolution Infrared Radiation Sounder (HIRS/2) with 19 infrared (IR) spectral channels between 3.7 and 15 μm and one visible (VIS) channel (0.7 μm) and the Microwave Sounding Unit (MSU) with four microwave channels around 5 mm. In order to convert these measured radiances into atmospheric properties, complex

inversion algorithms are necessary. At present, the TOVS Path-B dataset (Scott et al., 1999) provides eight years of atmospheric temperature profiles (in 9 layers) and water vapour profiles (in 4 layers) as well as cloud and surface properties at a spatial resolution of 1° latitude x 1° longitude. A fast line-by-line radiative transfer model (4A, Scott and Chédin, 1981) and a huge collection of radiosonde measurements of temperature, humidity and pressure that are grouped by atmospheric conditions are used to generate the Thermodynamic Initial Guess Retrieval (TIGR) database for the initial guess of the atmospheric temperature profile retrieval (Chédin et al., 1985; Chevallier et al., 1998).

Clouds are detected at HIRS spatial resolution (17 km at nadir) by a succession of threshold tests, which depend on the simultaneous MSU radiance measurements that probe through the clouds. To insure more coherence with the MSU spatial resolution (~100 km at nadir), the HIRS radiances are averaged separately over clear pixels and over cloudy pixels within 100 km x 100 km regions. Average cloud-top pressure and effective cloud emissivity over cloudy pixels are obtained from four radiances in the 15 μm CO_2 absorption band (with peak responses from 400 to 900 hPa levels in the atmosphere) and one in the 11 μm IR atmospheric window by minimizing a weighted χ^2 (Stubenrauch et al., 1999c). The method is based on the coherence of the effective cloud emissivity, obtained from the five wavelengths at the pressure level of the real cloud. The cloud-top temperature, T_{cld}, is determined from p_{cld} by using the retrieved atmospheric temperature profile.

Retrieval of mean effective ice crystal size and ice water path of large-scale semi-transparent cirrus and their regional and seasonal variation

The mean effective diameter, D_e, can be considered as an effective photon path of the ice crystal size distribution and is defined by (Mitchell, 2002):

$$D_e = \frac{3}{2}\frac{IWC_s + IWC_l}{\rho_i (P_s + P_l)} \qquad (1)$$

where ρ_i is the bulk density of ice and is assumed to have the value of 0.92 g cm^{-3}, IWC_s and IWC_l are the ice water contents, and P_s and P_l are the projected areas, corresponding to number densities of small and large particle modes, respectively.

The retrieval of mean effective ice crystal diameters, D_e, of cirrus as well as sensitivity studies have been described in detail by Rädel et al. (2003). The cirrus emissivity at 8 μm should be smaller than or equal to the one at 11 μm, depending on D_e. The emissivity difference is largest for small ice crystals (about 0.3 for D_e = 5 μm). It becomes negligible for ice crystal diameters of about 80 μm. Since the retrieval in the IR is mainly based on spectral absorption difference, it performs only for semi-transparent cirrus clouds (IR effective emissivity between 0.3 and 0.85 or visible optical thickness between 0.7 and 3.8).

Cirrus emissivities, ε, at 8.3 and 11.1 μm are computed from the measured brightness temperatures T_B^m, cloud-top temperature T_{cld} and surface temperature T_{surf}. To transform the retrieved cirrus emissivities into D_e, we compare them to look-up tables. These have been constructed from radiative transfer computations (Key and Schweiger, 1998) for a homogeneous ice cloud of 1 km thickness, with a top at 10 km, containing planar polycrystals distributed according a bimodal Γ-size distribution. The lapse rate is assumed as 6.5°C/km. Since the TOVS Path-B dataset provides simultaneous information on cloud properties and atmospheric profiles, we compute the cirrus emissivities by taking out atmospheric water vapour contributions from the measured radiances. Therefore, we can compare the cirrus emissivity difference between 8 and 11 μm to simulations not taking into account the atmosphere, contrary to approaches which use brightness temperature differences. The latter have to

be compared to simulations under a certain assumption of the underlying atmosphere.
To reduce the contribution of partly covered pixels, the ice crystal size retrieval is only performed for overcast high clouds (p_{cld} < 440 hPa), with all HIRS pixels cloudy over an area of 1° latitude x 1° longitude. The frequencies of these large-scale high clouds lie about 10 % below those of all high clouds. The D_e retrieval is influenced by the increase of pixel size and path of the emitted radiation received by the HIRS radiometer with viewing zenith angle. Therefore, we limit the D_e retrieval to cirrus clouds identified under a viewing zenith angle up to 25°.

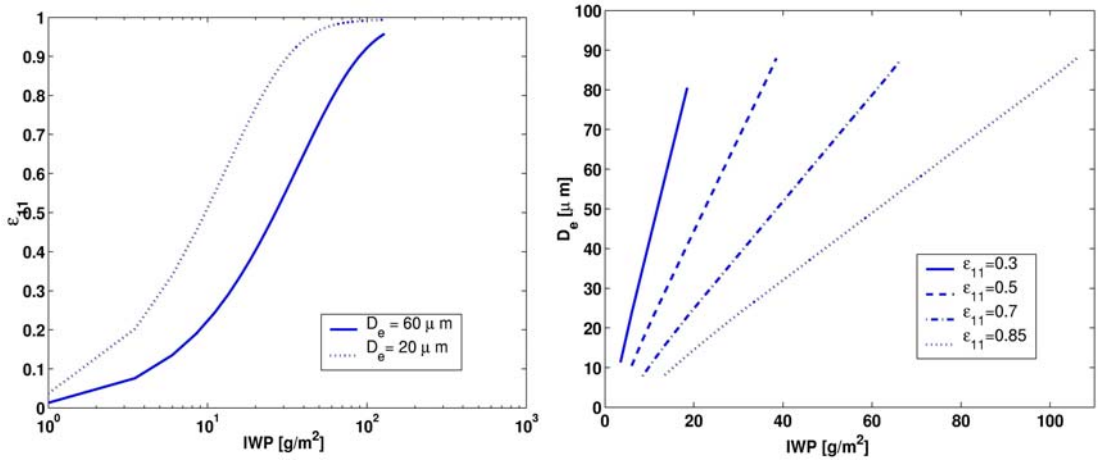

Fig. 1: a) Simulated cirrus emissivity at 11 μm, ε_{11}, as a function of ice water path, IWP, for two different mean effective ice crystal diameters D_e, and b) possible values of D_e and IWP for four distinct simulated cirrus emissivities.

Once D_e is retrieved from the cirrus emissivity difference between 8.3 and 11.1 μm, the ice water path (IWP) can be obtained from D_e and ε(11μm), because the emissivity is a function of IWP and D_e. Therefore, another set of look-up tables has been created from these simulations. Fig. 1a presents the cirrus emissivity at 11μm as a function of IWP, simulated for two mean effective ice crystal diameters. From this figure we deduce that the same cirrus emissivity (for example 0.6) can be reached by small D_e (20 μm) and IWP (10 gm^{-2}) or by large D_e (60 μm) and IWP (30 gm^{-2}). Fig. 1b shows which ranges of D_e and IWP can produce a given cirrus emissivity, using the same simulation. In the case of optically thin cirrus, D_e varies stronger within a small IWP range whereas in the case of optically thicker cirrus, D_e varies within a larger IWP range.

At present we have determined the mean effective ice crystal diameters and IWP of large-scale cirrus clouds NOAA10 TOVS observations. The cover the period from July 1987 until August 1991, with local observation times at 7h30 and 19h30.

Fig. 2 presents the seasonal variation of cirrus emissivity, cloud-top temperature, IWP and D_e, separately for ocean and land of the three latitude bands NH midlatitudes (30°N-60°N), tropics (20°N-20°S) and SH midlatitudes (30°S-60°S). IWP and D_e are on average the largest in the tropical region.

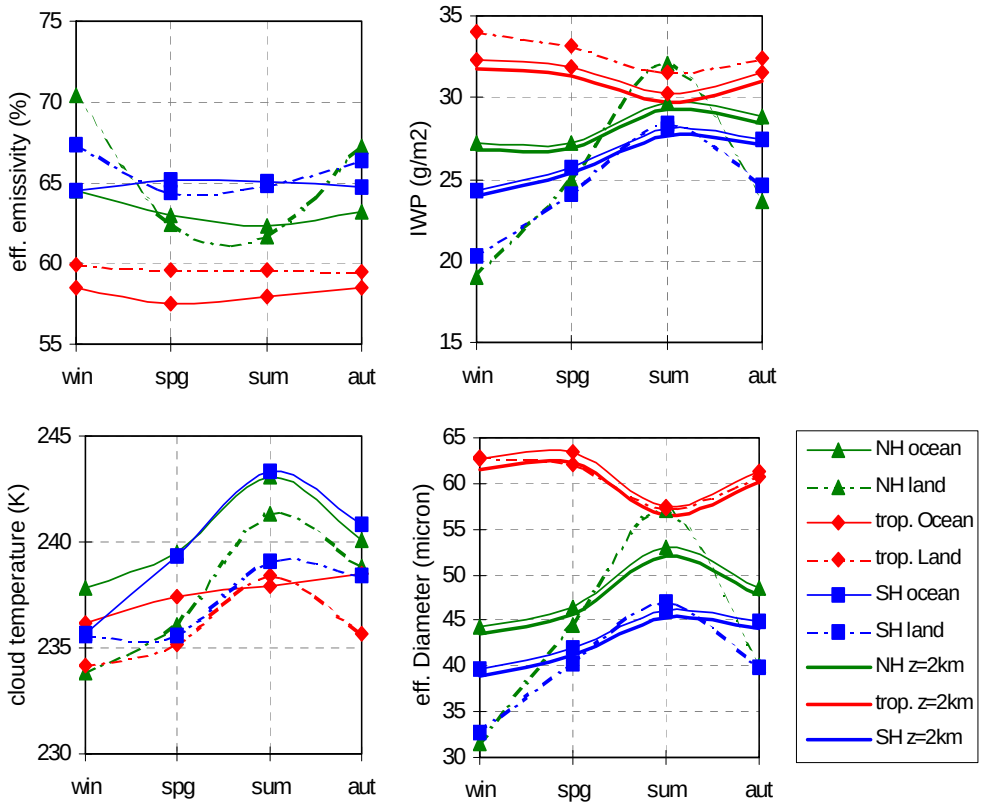

Fig. 2: Average cirrus emissivity (right), mean ice crystal diameter (middle) and IWP (left) of large-scale semi-transparent cirrus as function of season. Three-year averages over three latitude bands (Northern hemisphere midlatitude, tropics and Southern hemisphere midlatitude) are shown separately for land and ocean. Data were averaged using NOAA-10 TOVS observations from June 1987 until Mai 1990

From this figure we conclude the following:

- Large-scale semi-transparent cirrus have on average a smaller effective emissivity (0.57 over ocean and 0.60 over land) in the tropics than in the midlatitudes. However, their average IWP is larger (33 gm^{-2}) than the average IWP in the midlatitudes (28 gm^{-2} except summer). Their mean effective ice crystal diameter (60 µm) is then also larger than the average D_e in the midlatitudes (except during summer over NH land).

- Differences in cirrus emissivity between tropical ocean and land mainly result from differences in IWP.

- Large-scale semi-transparent cirrus in the tropics have no remarkable seasonal cycle in cirrus emissivity, IWP and D_e.

- Large-scale semi-transparent cirrus in the midlatitudes reveal a seasonal cycle, with larger IWP and D_e in Large-scale semi-transparent cirrus have on average a smaller effective emissivity (0.57 summer than in winter. The seasonal cycle of IWP and D_e is also stronger over land than over ocean. Cloud-top temperature in the midlatitudes is also higher in summer than in winter.

- Over ocean during all seasons, IWP and D_e are slightly larger in the Northern Hemisphere than in the Southern Hemisphere.

Since retrieved D_e and IWP can have biases linked to different assumptions (see Table 1 in Rädel et al. 2003), we have investigated the effect of doubling the cloud thickness (from 1 km to 2 km), by recalculating new look-up tables. These results, shown in addition in Fig. 2 for ocean, are very similar.

Correlations between D_e, IWP and T_{cld}

In many climate models D_e, and IWP are parameterised as functions of the cloud-top temperature $T_{cld.}$ Until now, these parameterisations were developed from restricted in-situ data. Fig. 3 presents the average D_e and IWP of all large-scale cirrus clouds between 60°N and 60°S as a function of T_{cld}.

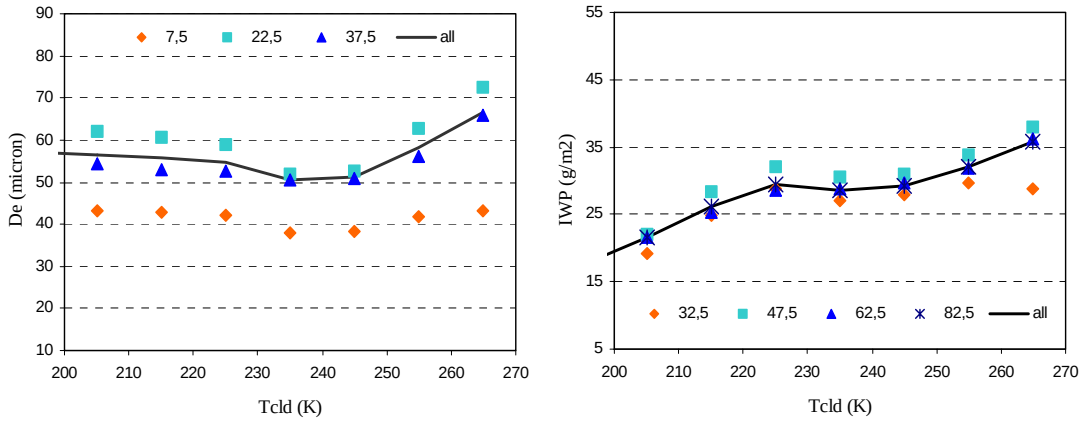

Fig. 3: Average mean ice crystal diameter D_e (left) and IWP (right) of large-scale semi-transparent cirrus as function of cloud temperature. The full line represent three-year averages over the globe from 60°N to 60°S. In addition, D_e averages are shown separately for three IWP intervals and IWP averages for four D_e intervals.

Whereas IWP increases steadily over the whole temperature range (from 200 K to 270 K) from 20 gm^{-2} to 35 gm^{-2}, the behaviour of D_e with cloud temperature is less clear. For cold temperatures (T_{cld} < 235 K), there is no dependence, while for warmer temperatures D_e increases slightly from 50 to 62 µm. The IWP also seems to change its slope slightly around T_{cld} of 235 K. This can be linked either to different processes of cloud formation (the probability of homogeneous freezing increases with decreasing temperature (e. g., Khain et al., 2000) or to the fact that at higher temperatures more water droplets are included in the cloud (e. g., Cober et al., 2001). The inclusion of water droplets would lead to a slight overestimation of D_e (Rädel et al., 2003; Yang et al., 2003).

We refine our analysis by studying separately three different IWP intervals and four different D_e .

The dependence of D_e and IWP on T_{cld} for the respective intervals is again shown in Fig. 3. One observes only a small scatter of IWP due to different D_e (about 5 gm^{-2}), whereas the scatter of D_e due to different IWP is large (up to 30 µm) and is certainly larger than the dependence on T_{cld}.

Figs. 4 show the dependence of D_e and IWP on T_{cld} for midlatitude summer and tropics. Midlatitude winter is not shown but shows similar behaviour as midlatitude winter. From these figures we conclude:

- D_e of large-scale semi-transparent cirrus varies in all regions more with IWP than with T_{cld}

- IWP of these cirrus increases steadily with T_{cld} in the midlatitudes , whereas in the tropics this behaviour is valid only for T_{cld} < 235K and the increase is faster for smaller D_e

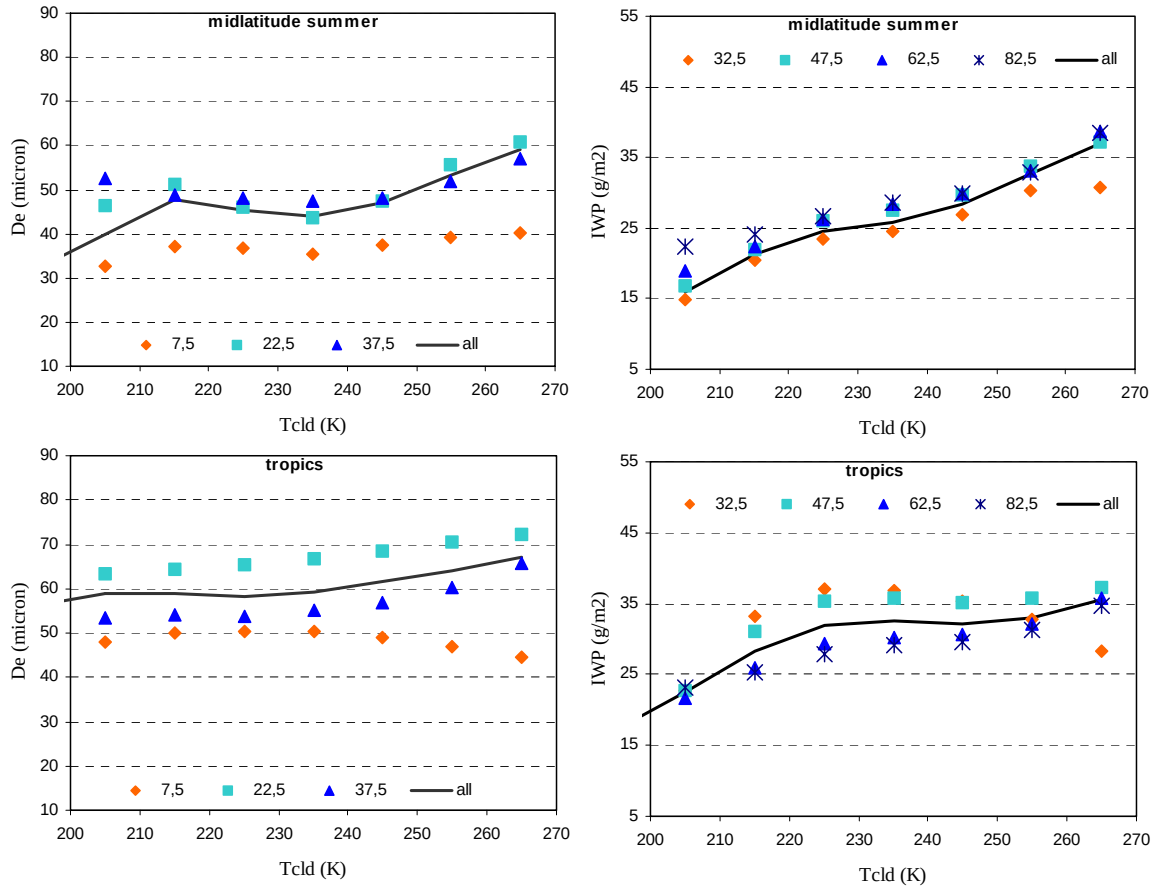

Fig. 4: Average D_e (left) and IWP (right) of large-scale semi-transparent cirrus as function of cloud temperature, separately for midlatitude summer and tropics. The full lines represent three-year averages. In addition, D_e averages are shown separately for three IWP intervals and IWP averages for four D_e intervals.

Field campaigns often measure microphysical properties of specific types of cirrus. Therefore we separated the large-scale cirrus into those with a relatively small effective emissivity ($0.30<\varepsilon(11\mu m)<0.55$) and those with a relatively large effective emissivity ($0.55<\varepsilon(11\mu m)<0.80$). As can be expected from Figs. 1a and 1b, we observe on average lower IWP values in the case of optically thin clouds than in the case of optically thicker clouds. It is interesting to note that D_e of optically thin cirrus is on average larger than D_e of optically thick clouds. The spread of D_e and IWP due to different IWP (and D_e) is slightly larger for optically thin cirrus than for optically thicker cirrus (40 µm (10 gm^{-2}) and 30 µm (7 gm^{-2}), respectively). For both types of cirrus, there is no dependence of D_e on T_{cld} for cold temperatures. For large-scale cirrus with $\varepsilon_{cld} > 0.55$ the spread of D_e and IWP due to different IWP (and D_e) is much smaller in the tropics than in the midlatitudes. This will be investigated further in the next section, by introducing dynamical parameters of the atmosphere.

Atmospheric properties related to large-scale semi-transparent cirrus

The ECMWF reanalysis ERA-40 (e.g. Courtier et al., 1998; Andersson et al., 1998) is based on the Integrated Forecast System and makes use of historical ground-based observations (components of the

Word Weather Watch by the World Meteorological Organization) as well as of multi-channel satellite radiances (from TOVS) through a three dimensional variational assimilation. It also includes a one dimensional variational assimilation of total column water content and surface wind speed using the Special Sensor Microwave / Imager (SSM/I) data. Cloud motion winds are integrated from geostationary satellite observations. At the end of the processing, the period covered should be about 40 years, from mid-1957 to 2002. The ERA-40 reanalysis provides, among other parameters, temperature, humidity, vertical and horizontal winds within grids of 1.125° latitude x 1.125° longitude. Vertical Pressure levels are given at intervals of 75 hPa between 1000 and 700 hPa, of 100 hPa between 700 and 300 hPa and of 50 hPa between 300 and 100 hPa. The temporal resolution is six hours, with data at the same universal time.

To study correlations between cirrus bulk microphysical properties of large-scale semi-transparent cirrus and the humidity and dynamics of the atmosphere in which they are embedded, we couple the TOVS Path-B cirrus data with the most coincident ERA-40 data (less than 6 hours before and less than 50 km apart). The vertical (w) and horizontal winds (u,v) are chosen to be in the closest vertical pressure level underneath the cirrus. The horizontal wind has been computed from the South-North (v) and West-East components (u) as $uv = \sqrt{(u^2+v^2)}$. For the following analysis, we have coupled ERA-40 data with TOVS Path-B data for summer (June to August) and winter (December to February) of 1989 and 1990.

Average atmospheric properties related to large-scale semi-transparent cirrus in NH midlatitudes, tropics and SH midlatitudes.

	Water vapour (cm)		Horizontal wind (m/s)		Frequency of situations with		
	mean	RMS	mean	RMS	updraft	no wind	downdraft
NHmidlatitude summer	3.0	1.2	14.5	10.9	9%	38%	3%
NH midlatitude winter	1.4	0.8	26.1	15.8	13%	29%	7%
tropics	5.0	0.9	7.6	6.0	7%	44%	0.1%
SH midlatitude summer	2.3	1.0	23.4	13.8	6%	42%	4%
SH midlatitude winter	1.5	0.8	22.3	15.2	10%	34%	4%

Table 1 gives an overview of atmospheric properties in the three latitude bands NH midlatitudes, tropics and SH midlatitudes, when large-scale cirrus are present. For the midlatitudes, average properties are shown for summer and winter separately. As expected, total atmospheric water vapour is highest in the tropics and lowest in midlatitude winter. Horizontal wind at cloud level is on average weakest in the tropics and strongest in NH midlatitude winter. In the southern hemisphere, horizontal winds are strong in winter and in summer. Vertical wind can appear as updraft or as downdraft. To investigate vertical wind, we therefore compute frequencies of occurrence of situations with strong large-scale updraft ($w < -0.2$ Pa/s), very weak vertical wind ($|w| < 0.05$ Pa/s), and strong large-scale downdraft ($w > 0.2$ Pa/s), all averaged over 1.125° latitude x 1.125° longitude. At this spatial resolution, the vertical wind in the tropics is often weak, in 7% of the large-scale cirrus situations there is a strong updraft, there are nearly no downdraft situations. In the midlatitudes, there are more situations with a large updraft in winter than in summer.

Correlations between D_e, IWP, atmospheric humidity and winds

To understand the dependence of D_e and IWP of large-scale cirrus on all these atmospheric

properties, we study mean D_e and IWP as function of atmospheric humidity, in the case of four different dynamic situations: no winds (|w| < 0.05 Pa/s and uv < 20 m/s), strong vertical updraft (w < -0.2 Pa/s and uv < 20 m/s) only, strong horizontal wind only (|w| < 0.05 Pa/s and uv > 35 m/s), and strong vertical updraft and horizontal wind (w < -0.2 Pa/s and uv > 35 m/s), as presented in Figs. 5 for cold large-scale cirrus (T_{cld} < 233 K) over the globe (60°N-60°S).

On global average IWP, as well as D_e of these cold, large-scale cirrus are larger in a humid than in a dry atmosphere. In humid situations, IWP is about 10 gm^{-2} larger in regions with strong large-scale vertical updraft than in regions with strong horizontal winds. The latter possibly increase the horizontal cirrus extent and therefore decrease on average the IWP.

Also the mean effective ice crystal size seems to depend on the large-scale dynamical situation, especially in humid air: D_e is about 10 μm larger in case of no large-scale winds than in case of strong large-scale winds. Vertical updraft seems to play a slightly bigger role in the decrease of D_e than horizontal wind.

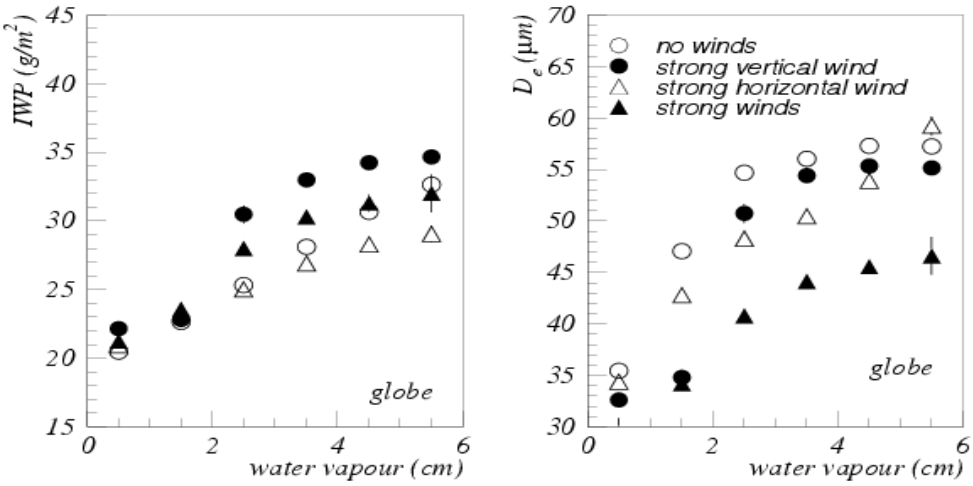

Fig. 5: Global average ice water path IWP (left) and mean ice crystal size D_e (right) of all cold, large-scale semi-transparent cirrus as function of atmospheric humidity, for four different dynamic situations: no winds (o), strong vertical updraft only (•), strong horizontal wind only (△), and strong horizontal wind and vertical updraft (▲)

Our large-scale observations show that in addition to temperature also atmospheric water vapour and winds play a role in the distribution of bulk microphysical properties of cirrus.

It is difficult to compare these results to in-situ data, because the horizontal wind has not been measured or analysed and only ice crystal concentrations (and not IWP) have been analysed in studies which have connected cirrus bulk microphysical properties to vertical updraft (Stith et al., 2002; Kärcher and Ström, 2003).

Conclusions and outlook

In addition to cirrus physical properties, such as cloud-top temperature and effective cloud emissivity, the TOVS instruments also allow to retrieve their mean effective ice crystal diameters, integrated over the cloud depth, and then their IWP. Since the D_e retrieval method is essentially based on the spectral difference in absorption, it can only be applied to semi-transparent cirrus (ε_{IR} < 0.85 or τ_{VIS} < 3.8). The method is sensitive to diameters up to 80 μm, and to avoid too much horizontal heterogeneity and too much influence from the atmosphere below, it is applied to large-scale (covering at least 1° latitude x 1° longitude) semi-transparent cirrus with ε_{IR} > 0.3 or τ_{VIS} > 0.7. The global

averages (from 60°N to 60°S) of D_e and IWP of these clouds are 55 µm and 30 gm^{-2}, respectively. IWP and D_e are on average larger in the tropics than in the midlatitudes, where they are larger during summer than during winter.

Correlations between average D_e, IWP and cloud-top temperature of semi-transparent cirrus over the globe have been investigated. IWP was found to increase steadily over the whole temperature range (from 200 K to 270 K) from 20 gm^{-2} to 35 gm^{-2}. However, the behaviour of D_e, with cloud-top temperature is not so clear. For cold temperatures (T_{cld} < 235 K), there is no dependence, whereas for warmer temperatures mean D_e increases slightly. On the other hand, the scatter of D_e due to different IWP is large (up to 30 µm) and is certainly larger than the dependence on T_{cld}. In addition correlations are different for optically thicker or thinner cirrus, and depending on the latitude.

By making use of TOVS Path-B satellite retrievals and ECMWF reanalyses, we could analyze for the first time correlations between bulk microphysical properties of large-scale semitransparent cirrus and thermodynamic and dynamic properties of the surrounding atmosphere.

On global average, IWP as well as D_e of cold large-scale cirrus are larger in a humid than in a dry atmosphere. In humid situations, IWP is about 10 gm^{-2} larger in regions with strong large-scale vertical updraft than in regions with strong horizontal winds. The latter possibly increase the horizontal cirrus extent and therefore decrease on average the IWP.

Also the mean effective ice crystal size seems to depend on the large-scale dynamical situation, especially in humid air: D_e is about 10 µm larger in case of no large-scale winds than in case of strong large-scale winds. Differences between midlatitudes and tropics suggest that dynamical and thermodynamical parameters of the atmosphere are very important for the resulting bulk microphysical properties of cirrus, in addition to formation process. In the tropics, most large-scale semitransparent cirrus are part of anvils of tropical convection, whereas in the midlatitudes these clouds are related to jet streams and weather fronts.

This study was performed in the framework of the European project CIRAMOSA (http://www.lmd.polytechnique.fr/CIRAMOSA/Welcome.html) and will be published in more detail in Stubenrauch et al. 2004.

In a next step, we will try to find parameterizations of IWP as a function of water vapour, vertical updraft, horizontal wind and T_{cld} as well as D_e as a function of water vapour, vertical updraft, horizontal wind and IWP. These parameterizations could be used in climate models for the computation of radiative fluxes of cirrus clouds, until cloud resolving models find more sophisticated parameterizations

References

Andersson, E., Haseler, J., Unden, P., Courtier, P., Kelly, G., Vasiljevic, D., Brankovic, C., Cardinali, C., Gaffard, C., Hollingsworth, A., Jakob, C., Janssen, P., Klinker, E., Lanzinger, A., Miller, M., Rabier, F., Simmons, A., Straus, B., Thépaut, J.-.N., Viterbo, P., 1998. The ECMWF implementation of three-dimensional variational assimilation (3D VAR). III: Experimental results. *J. Roy. Meteor. Soc.*, **124**, 1831-1860.

Chédin, A., Scott, N. A., Wahiche, C., Moulinier, P., 1985. The Improved Initialized Inversion method: A high resolution physical method for temperature retrievals from the TOVS-N series. *J. Climate Appl. Meteor.*, **24**, 128-143.

Chevallier, F., Chéruy, F., Scott, N. A., Chédin, A., 1998. A neural network approach for a fast and accurate computation of a longwave radiative budget. J. Appl. Meteor. 37, 1385-1397.

Cober, S.G., Isaac, G.A., Korolov, A.V., Strapp, J. W., 2001. Assessing Cloud-Phase Conditions. *J. Appl. Meteor.* , **40**, 1967-1983.

Courtier, P., Andersson, E., Heckley, W., Pailleux, J., Vasiljevic, D., Hamrud, M., Hollingsworth, A., Rabier, F., Fisher, M., 1998. The ECMWF implementation of three-dimensional variational assimilation (3D-

VAR). I: Formulation. *Quart. J. Roy. Meteor. Soc*., **124**, 1783-1807.
Donner, L. J., C. J. Seman, B. J. Soden, R. S. Hemler, J. C. Warren, J. Ström, and K.-N. Liou, 1997: Large-scale ice clouds in the GFDL SKYHI general circulation model. *J. Geophys. Res.*, **102**, 21745-21768.
Heymsfield, A. J., 1977. Precipitation development in stratiform ice clouds: A microphysical and dynamical study. *J. Atmos. Sci.* , **34**, 367-381.
Heymsfield, A. J., Platt, C. M. R., 1984. A parameterization of the particle size spectrum of ice clouds in terms of the ambient temperature and the ice water content. *J. Atmos. Sci.*, **41**, 846-855.
Kärcher, B., Ström, J., 2003. The roles of dynamical variability and aerosols in cirrus cloud formation. *Atmos. Chem. Phys. Discuss.*, **3**, 1415-1451.
Key, J., Schweiger, A., 1998. Tools for atmospheric radiative transfer: Streamer and FluxNet. *Computer & Geosciences*, **24**, 443-451.
Khain, A., Ovtchinnikov, M., Pinsky, M., Pokrovsky, A., Krugliak, H., 2000: Notes on the state-of-the-art numerical modelling of cloud microphysics. *Atmos. Res.*, **55**, 159-224.
Korolev, A. V., Isaac, G. A., Mazin, I. P., Barker, H. W., 2001. Microphysical properties of continental clouds from in-situ measurements. *Quart. J. Roy. Meteor. Soc*. ,**127**, 2117- 2151.
Kristjansson, J. E., Edwards, J. M., Mitchell, D. L., 1999. A new parameterization scheme for the optical properties of ice crystals for use in general circulation models of the atmosphere. *Phys. Chem. Earth* **B 24**, 231-236.
Kristjansson, J. E., Edwards, J. M., Mitchell, D. L., 2000. Impact of a new scheme for optical properties of ice crystals on climates of two CGM's. *J. Geophys. Res.*, **105**, 10063-10079.
McFarlane, N. A., Boer, G. J., Blanchet, J. P., Lazare, M., 1992. The Canadian Climate Centre second-generation general circulation model and its equilibrium climate. J. Climate 5, 1013-1044.
McFarquhar, G. M., Heymsfield, A. J., 1996. Microphysical Characteristics of three Anvils sampled during the Central Equatorial Pacific Experiment (CEPEX). *J. Atmos. Sci.* , **53**, 2401-2423.
Mitchell, D. L., 2002. Effective diameter in radiative transfer: Definition, applications and limitations. *J. Atmos. Sci.*, **59**, 2330-2346.
Rädel, G., Stubenrauch, C. J., Holz, R., Mitchell, D. L., 2003. Retrieval of Effective Ice Crystal Size in the Infrared : Sensitivity Study and Global Measurements from the TIROS-N Operational Vertical Sounder. *J. Geophys. Res.*, **108**, D9 4281-4292..
Smith, W. L., Woolf, H. M., Hayden, M. C., Wark, D. Q., McMillin, L. M., 1979. The TIROS-N Operational Vertical Sounder. *Bull. Amer. Meteor. Soc.* , **60**, 1177-1187.
Scott, N. A., Chédin, A., 1981. A fast line by line method for atmospheric absorption computations: the Automized Atmospheric Absorption Atlas. *J. Appl. Meteor.*, **20**, 802-812.
Scott, N. A., Chédin, A., Armante, R., Francis, J., Stubenrauch, C. J., Chaboureau, J.-P., Chevallier, F., Claud, C., Chéruy, F., 1999. Characteristics of the TOVS Pathfinder Path-B Dataset. *Bull. Amer. Meteor. Soc.*, **80**, 2679-2701.
Stith, J. L., Dye, J. E. Bansemer, A., Heymsfield, A. J., Grainger, C. A., Petersen, W. A. , Cifelli, R., 2002. Microphysical observations of tropical clouds. *J. Appl. Meteor*., **41**, 97-117.
Stubenrauch, C. J., Rossow, W. B., Scott, N. A., Chédin, A., 1999a. Clouds as seen by Infrared Sounders (3I) and Imagers (ISCCP): Part III) Combining 3I and ISCCP Cloud Parameters for better Understanding of Cloud Radiative Effects. *J. Climate*, **12**, 3419-3442.
Stubenrauch, C. J., Holz, R., Chédin, A., Mitchell, D. L., Baran, A. J., 1999b. Retrieval of Cirrus Ice Crystal Sizes from 8.3 and 11.1 μm Emissivities Determined by the Improved Initialization Inversion of TIROS-N Operational Vertical Sounder Observations. *J. Geophys. Res*., **104**, 31793-31808.
Stubenrauch, C. J., A. Chédin, R. Armante, and N. A. Scott, 1999c: Clouds as seen by Infrared Sounders (3I) and Imagers (ISCCP): Part II) A New Approach for Cloud Parameter Determination in the 3I Algorithms. *J. Climate*, **12**, 2214-2223.
Stubenrauch, C. J., Eddounia, F., Rädel, G., 2004. Correlations between microphysical properties of large-scale semi-transparent cirrus and the state of the atmosphere. To appear in *Atmos Res.*.
Wylie, D. P., Menzel, W. P., Woolf, H. M., Strabala, ,K. I., 1994. Four Years of Global Cirrus Cloud Statistics using HIRS. J. Climate 7, 1972-1986.
Wylie, D.P., Menzel, W.P., 1999. Eight Years of High Cloud Statistics Using HIRS. J. Climate 12, 170-184.
Yang, P., Wei, H.-L., Baum, B., Huang, H.-L., Heymsfield, A. J., Hu, Y. X., Gao, B.-C., Turner, D. D., 2003. The spectral signature of mixed-phase clouds composed of non-spherical ice crystals and spherical liquid droplets in the terrestrial window region. J. Quant. Spectros. Rad. Trans. 79-80, 117.